Available online at www.sciencedirect.com

SciVerse ScienceDirect

journal homepage: www.elsevier.com/locate/he

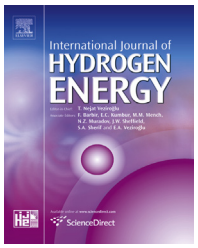

Heterostructured (Ba,Sr)TiO_3/TiO_2 core/shell photocatalysts: Influence of processing and structure on hydrogen production

*Li Li, Xuan Liu, Yiling Zhang, Paul A. Salvador, Gregory S. Rohrer**

Department of Materials Science and Engineering, Carnegie Mellon University, 5000 Forbes Ave., Pittsburgh, PA 15213, USA

ARTICLE INFO

Article history:
Received 22 January 2013
Received in revised form
23 March 2013
Accepted 25 March 2013
Available online 24 April 2013

Keywords:
Core/shell
Photocatalyst
TiO_2
Internal fields
Nano/micron heterostructure

ABSTRACT

Heterostructured powders composed of microcrystalline (*mc*-) $BaTiO_3$ and $SrTiO_3$ cores coated with nanostructured (*ns*-) TiO_2 shells were prepared using a sol–gel method. The influences of annealing temperature, coating thickness, cocatalyst loading, and core size on photocatalytic hydrogen production were experimentally determined. The amount of hydrogen produced depends on the annealing temperature, which influences the interface, phase composition, light absorption, crystallinity, mesoporosity, and surface area. The heterostructured powders produced more hydrogen than *ns*-TiO_2 alone when annealed between 500 °C and 800 °C. The amount of hydrogen produced by heterostructures with 100–150 nm thick nanostructured titania coatings was greater than for thicker or thinner coatings. The optimum Pt loading was determined to be 1% by weight. Heterostructured powders consisting of *mc*-$BaTiO_3$/*ns*-TiO_2 produce more hydrogen than those with nano-sized $BaTiO_3$ cores, suggesting a size effect that is counter to the conventional relationship between catalytic activity and particle size.

1. Introduction

Particulate photocatalysts for water splitting have the advantage of being low in cost when compared with photoelectrochemical cells. However, the low efficiency of particulate photocatalysts remains a major constraint on their applicability. In general, powdered titania photocatalysts absorb only a small fraction of solar light, and then only a small percentage of the charge carriers created by absorbed photons are used for photolysis [1]. Nanoscale powder photocatalysts are of interest because they maximize the reactive surface area. However, nanoscale powders cannot fully support internal space charges, which are beneficial to charge separation [2]. Also, because the photogenerated charge carriers and reaction products are produced in close proximity, carrier recombination and back-reaction of intermediates can be enhanced. These losses are considered major bottlenecks to photocatalytic hydrogen production [3].

To reduce the rates of back reaction and charge carrier recombination, cocatalysts [4,5], semiconductor junctions [6,7], and modifications of the crystal structure and morphology [8–11] have been studied. Motivated by the fact that photoelectrochemical cells use the internal voltage at the semiconductor–solution interface to spatially separate the charge carriers and redox reactions, recent research has attempted to exploit internal fields in heterostructured semiconductor particles to increase efficiency. In such structures, it is important to control the length scales of the structural features in each phase to optimize light absorption and charge carrier separation, as well as reactive surface area. The main goal of this work is to provide experimental guidance for the control of these length scales in heterostructured

* *Corresponding author*. Tel.: +1 412 268 2696; fax: +1 412 268 7596.
E-mail address: gr20@andrew.cmu.edu (G.S. Rohrer).
0360-3199/$ – see front matter
http://dx.doi.org/10.1016/j.ijhydene.2013.03.130

powders and to demonstrate that combining nano- and micro-scale powders can be advantageous toward these ends.

Using planar heterojunctions, it has been shown that internal fields in oxide semiconductors affect photochemical reactions [12–17]. These fields can originate from dipolar fields from ferroelectrics, band offsets, or trapped charge at the interface. The concepts demonstrated in these planar heterostructures have been extended to high surface area powders, in which nanostructured titania is used in conjunction with a microcrystalline support. For example, high surface area titania supported by tourmaline was used for water splitting [18], sol–gel derived titania supported by $FeTiO_3$ [19] and $PbTiO_3$ [20] showed visible light activity for dye degradation, and sol–gel derived titania supported by $BaTiO_3$ and $SrTiO_3$ showed enhanced activity for photocatalytic hydrogen production [21]. In each of these cases, the length scales and structural characteristics of the core–shell architecture are expected to influence the reaction. For example, the internal field within the core material is thought to influence band bending at the core/shell interface and promote the separation of photogenerated charge carriers. The micron-sized core is necessary to provide the appropriate length scale for band bending and light absorption [22,23]. On the other hand, photochemical reactions occur in the nanostructured TiO_2. The high surface area of nanostructured TiO_2 provides abundant active sites to catalyze photochemical reactions.

While the efficacy of heterostructured catalysts for photochemical reactions has been demonstrated [18–21], the influence of the different length scales has not been systematically explored. The purpose of the present paper is to determine how different annealing temperatures, different coating thicknesses, cocatalyst loadings, and core sizes affect the rate of photocatalytic hydrogen production from nanostructured TiO_2 supported by a microcrystalline core. As an example, we focus on $SrTiO_3$ and $BaTiO_3$ supports that were previously shown to enhance the photocatalytic properties of nanostructured titania [21]. The results indicate that there are optimal length scales in the design of heterostructured photocatalysts. For example, heterostructured catalysts having nanoscale titania shells and large (micron-sized) cores produce more hydrogen than those with nano-scale cores, in spite of the decreased reactive surface areas and decreased interfacial areas. Also, the optimal thickness of the nanoscale core is observed to be between 100 and 150 nm, indicating that there is a balance between the increased total surface area per particle of the nanostructured shell and the expected decrease in reactivity of the coating with increased thickness. These observations indicate that the control of structure at all length scales in heterostructured photocatalytic powders is essential to maximize their photocatalytic properties.

2. Experiment

2.1. *Photocatalyst processing*

Microcrystalline cores of barium titanate ($BaTiO_3$, Alfa Aesar, 99.7%) and strontium titanate ($SrTiO_3$, Acros Organics, >99%) were obtained commercially. Before using them as cores, the powders were treated in molten KCl. The KCl was used as a low-melting temperature inorganic flux, in which $BaTiO_3$ or $SrTiO_3$ can coarsen through dissolution and precipitation. This process produces particles with flatter surfaces and faceted shapes, as previously demonstrated [24,25]. Equal weights of $BaTiO_3$ and KCl (Acros Organics, >99%) were mixed and ball milled with ethanol for 5 min and stirred for 2 h to guarantee the uniform dispersion of the components. The dried powders were heated to 1100 °C (where the KCl is molten) for 5 h with a 5 °C/h heating rate. The KCl was then removed with boiling water. The powder was dried at 70 °C and then collected for the coating process.

The $BaTiO_3$ and $SrTiO_3$ described above were coated with nanostructured titania by the hydrolysis of TBOT ($Ti(OC_4H_9)_4$, ACROS ORGANICS, 99.0%) [26,27]. The experimental details have already been reported [21]. The core materials were suspended in a solution of water (9 mL) and ethanol (20 mL) after dispersion by sonication and stirring for 0.5 h. HCl was used to adjust the pH to the range of 3–4. Another solution (denoted as TBOT solution) containing ethanol (15 mL), TBOT (8.6 mL), and 2,4-pentanedione (1 mL) was added drop-wise into the solution of suspended core materials. The mixture was stirred vigorously for 2 h and was aged at 90 °C in a water bath for 9 h while stirring at 300 rpm. During this process, some of the titania forms on the cores and some remains suspended in solution. Thus, the suspension was centrifuged so that the denser coated particles could be separated from the free titania and excess TBOT in the supernate. The titania:core mass faction in the starting materials was 1.2:1, but, because only a fraction of this forms on the cores, the titania:core mass fraction of the heterostructured particles is lower. After centrifugation and separation, the precursor was washed with ethanol and dried at 80 °C for 24 h for the formation of the xerogel. The xerogel was then transferred to an Al_2O_3 crucible and calcined to crystallize the TiO_2 by heating at 5 °C/h to various temperatures between 400 °C and 900 °C. The final product was obtained after calcination. Commercial nanostructured (*ns*-) $BaTiO_3$ (US Research Nanomaterials, 99.9%), with a crystal size of ≈100 nm (measured by SEM), was coated with *ns*-TiO_2 using the same procedure as for the *mc*-$(Ba,Sr)TiO_3$/*ns*-TiO_2 heterostructured powders. Nanostructured TiO_2 powders were obtained following the same procedure discussed above, but without the addition of micron-sized core materials.

The thicknesses of the coating on the heterostructured *mc*-$BaTiO_3$/*ns*-TiO_2 powders were varied by using multiple coating cycles. After the precursor was dried, the xerogel was ground into fine powders with a porcelain mortar and pestle and was then dispersed into another TBOT solution for a repeated coating process. The xerogel produced from 1, 2, or 3 coating cycles was then heated at 5 °C/min to 500 °C and calcined for 2 h to crystallize the TiO_2 shell. The final powders obtained from this procedure were denoted as BT-1, BT-2, and BT-3 for powders coated 1, 2, or 3 times, respectively. While the coating thickness could be controlled in other ways, such as changing the concentration of TBOT or the pH of the precursor, multiple coating steps were used as a simple method that maintains consistent processing conditions between dissimilar samples, minimizing the differences in the structure that results from the processing history.

An impregnation-reduction method was used to load all powders with Pt to act as a cocatalyst [28,29]. The as-prepared powders were impregnated with a known quantity of H_2PtCl_6 solution for 2 h with stirring. The powders with adsorbed H_2PtCl_6 were reduced using a 5-fold excess of NaOH and $NaBH_4$ for 2 h with stirring. The powders were then collected by centrifugation, rinsed with distilled water, and dried at 70 °C for 12 h. To test the influence of the amount of cocatalyst on the photocatalytic activity of the heterostructures, samples of *mc*-$SrTiO_3$/*ns*-TiO_2 annealed at 600 °C were loaded with 0.1, 0.5, 1 and 2 wt% Pt, respectively. All other samples were loaded with 1 wt% Pt. While it should be noted that not all of the Pt is expected to precipitate on the powders, we will still refer to samples by the nominal composition of the starting materials.

2.2. Materials characterization

The phase composition of powders was analyzed by X-ray diffraction (XRD) using an X-ray diffractometer (PANalytical, X'Pert Pro, Philips, Netherlands) equipped with a high-intensity (45 kV, 45 mA) CuKα radiation source ($\lambda = 1.5406$ Å). θ–2θ diffraction patterns were collected from $2\theta = 20°$ to $2\theta = 90°$, using a scan rate of 3°/minute and a step size of 0.05°. Nitrogen adsorption/desorption measurements (Nova 2200e, Quantachrome, FL) were carried out at 77 K after the sample was vacuum-degassed for 3 h at 300 °C to remove moisture. The BET method was used to determine the surface area from the adsorption measurement at low relative pressures ($0.05 < P/P_0 < 0.3$). The mean pore size and volume were determined from the same measurements using the Barret–Joyner–Halenda (BJH) model (measured at the $P/P_0 = 0.99$ point). The morphologies of the powders were characterized by transmission electron microscopy (TEM) (F20, TECNAI, Hillsboro, OR) under an accelerating voltage of 200 kV with a field emission gun.

High resolution TEM images (HRTEM) were taken to observe the crystal lattice fringes of the TiO_2 coatings. For the preparation of TEM samples, powders were dispersed ultrasonically in methanol. Several drops of the suspension were then added drop-wise onto the surface of a 200 mesh copper grid coated with a holey carbon support film. The TEM was equipped with an energy dispersive X-ray spectrometer (EDS) for elemental analysis that was used to determine the coating composition. The EDS was operated in the high resolution scanning transmission electron microscopy (STEM) mode.

2.3. Photocatalytic experiment setup

The amount of photocatalytic hydrogen produced by the catalysts was measured by gas chromatography (GC) (Shimadzu, MD; GC-14A, Molecular Sieve 5Å Column, TCD) with Ar as the carrier gas. The photocatalytic activities of powders were evaluated by the amount of hydrogen generated in a fixed amount of time. The powders (0.4 g) were suspended in a 100 mL water/methanol (92/8 mL) mixture, contained within a gas-tight reactor system, and illuminated by a 450 W medium-pressure mercury immersion lamp (ACE Glass, NJ). The lamp was inserted into a borosilicate immersion well (ACE Glass, NJ) to allow the transmittance of irradiation with wavelengths larger than 280 nm. Methanol was used as a sacrificial reagent to promote hydrogen evolution [9,30]. The reaction system was evacuated prior to irradiation to establish a pressure below 5 torr inside the chamber. The photocatalytic reactor was water cooled so that the reaction took place at room temperature. Gas in the reactor was sampled each hour with a 0.5 mL syringe and analyzed by GC. As a control, the same photocatalytic experiment was performed without irradiation and no hydrogen was detected.

3. Results

3.1. Effect of annealing temperature

The phase composition of platinized TiO_2 annealed at different temperatures was determined by XRD. The XRD patterns of sol–gel fabricated TiO_2 annealed at 400, 500, and 600 °C (denoted as T-400, T-500, and T-600) are shown in Fig. 1-(a). At higher annealing temperatures, the intensity of

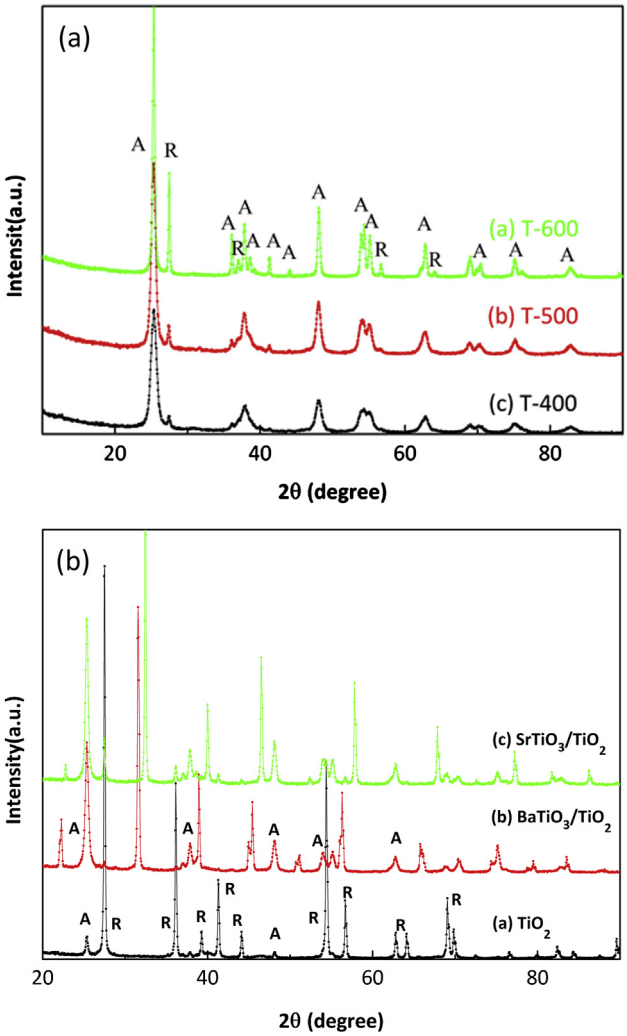

Fig. 1 – Comparison of powder X-ray diffraction patterns of (a) platinized TiO_2 annealed at 400–600 °C and (b) platinized $BaTiO_3/TiO_2$, $SrTiO_3/TiO_2$, and TiO_2 annealed at 700 °C. (T-400 represents TiO_2 annealed at 400 °C, etc; A and R refer to anatase and rutile TiO_2.)

the anatase peaks, denoted as A, decreases, as the intensity of the rutile peaks, denoted as R, increases. The conversion of anatase to rutile at high temperature is expected [31–33]. It has been reported that anatase converts to rutile at temperatures between 500 and 600 °C [34,35].

The X-ray diffraction patterns of platinized (1 wt%) $BaTiO_3/TiO_2$, $SrTiO_3/TiO_2$, and TiO_2 annealed at 700 °C are shown in Fig. 1-(b). All diffraction peaks can be indexed as $BaTiO_3$ (JCPDS 05-0626), $SrTiO_3$ (JCPDS 35-734), anatase (JCPDS 46-1237), and rutile (JCPDS 33-1381) TiO_2. The primary phase in the TiO_2 powder annealed at 700 °C is rutile. Several small peaks can be indexed as anatase. On the other hand, the primary phase for the TiO_2 shells in the $BaTiO_3/TiO_2$ and $SrTiO_3/TiO_2$ powders annealed at 700 °C is anatase. This result indicates that the core materials stabilize anatase in the nanostructured coating. This discovery is encouraging for photocatalytic hydrogen production because anatase is reported to have reduced carrier recombination rates compared to rutile [36]. The heterostructures can be processed at higher annealing temperatures to improve crystallinity, while still remaining in the anatase phase.

The rutile phase fraction was calculated using the following equation (assuming randomly oriented crystallites) [37]:

$$R\% = 1/(1+1.265I_A/I_R)$$

where R% is the percentage of rutile, I_A is the intensity of the anatase (101) peak, and I_R is the intensity of the rutile (110) peak, respectively. The crystallite size of anatase and rutile TiO_2 was determined with Scherrer's equation [38].

The XRD results are summarized in Table 1 to show the influence of annealing temperature on the phase composition and TiO_2 crystallite size. TiO_2 and $BaTiO_3/TiO_2$ heterostructures were annealed at various temperatures from 400 °C to 800 °C, while $SrTiO_3/TiO_2$ was annealed at temperatures from 500 °C to 900 °C. The conversion of anatase to rutile in TiO_2 starts in the range between 500 °C and 600 °C, and the transformation is mostly complete at 800 °C. The transformation of anatase to rutile in the $(Ba,Sr)TiO_3/TiO_2$ heterostructures begins in the range of 700 °C–800 °C, but at 800 °C the TiO_2 in the heterostructure is still more than half anatase. At any given temperature, the ratio of anatase TiO_2 in the $BaTiO_3/TiO_2$ heterostructure is slightly higher than that in the $SrTiO_3/TiO_2$ heterostructure, but the difference is relatively small. The transformation to rutile in the heterostructures is essentially complete (>97% rutile in $SrTiO_3/TiO_2$) at 900 °C.

Table 1 – The phase composition and TiO_2 grain sizes of $BaTiO_3/TiO_2$, $SrTiO_3/TiO_2$, and TiO_2 annealed at different temperatures. (A and R refer to anatase and rutile TiO_2.)

Catalyst	Annealing temperature (°C)	Anatase fraction (%)	TiO_2 grain size (nm)
TiO_2	400	91.6	10(A)
	500	89.9	13(A)
	600	77.5	27(A)
	700	5.6	48(R)
	800	0.4	50(R)
$BaTiO_3/TiO_2$	400	93.6	10(A)
	500	93.3	12(A)
	600	93.6	14(A)
	700	95.7	20(A)
	800	66.5	25(A) 40(R)
$SrTiO_3/TiO_2$	500	93.6	14(A)
	600	91.7	17(A)
	700	82.4	22(A)
	800	57.7	32(A) 44(R)
	900	2.8	50(R)

The XRD grain sizes for the primary TiO_2 phase are also given in Table 1 (with the exception of the heterostructures annealed at 800 °C, for which both anatase (A) and rutile (R) values are given). The size of anatase grains in TiO_2 and $(Ba,Sr)TiO_3/TiO_2$ are the same (10 nm) when annealed at 400 °C. With increased annealing temperature, the grain size of both anatase and rutile increased, presumably from thermal coarsening. The crystallite size of anatase in the TiO_2 powders increased from 10 nm to 27 nm when the annealing temperature increased from 400 °C to 600 °C. The crystallite size of rutile was 48 nm and 50 nm when annealed at 700 °C and 800 °C, respectively. At 800 °C, anatase shows a smaller grain size (25 nm in $BaTiO_3/TiO_2$ and 32 nm in $SrTiO_3/TiO_2$) than rutile (40 nm in $BaTiO_3/TiO_2$ and 44 nm in $SrTiO_3/TiO_2$), in accordance with the literature [36]. While they follow the same trends, the crystallite sizes of both anatase and rutile in the $(Ba,Sr)TiO_3/TiO_2$ heterostructures are smaller than those in the TiO_2 powders. This phenomenon indicates that the interaction of the TiO_2 coating with the core hinders coarsening. At any given temperature, the sizes of TiO_2 grains in the $BaTiO_3/TiO_2$ heterostructures are slightly smaller than those in the $SrTiO_3/TiO_2$ heterostructures, indicating that $BaTiO_3$ hinders coarsening slightly more than $SrTiO_3$, similar to $BaTiO_3$ retarding the phase transformation more than $SrTiO_3$. While the cause of this stabilizing effect was not studied here, it is known that perovskite substrates can epitaxially stabilize anatase thin films in conditions when rutile would normally be stable [13,14]. The same effect might decrease the driving force for coarsening and transformation in these heterostructured particles.

TEM bright field images of a platinized $SrTiO_3/TiO_2$ heterostructure annealed at 800 °C are shown in Fig. 2-(a) and (b). Fig. 2-(a) shows that the microcrystalline core is fully covered by the TiO_2 coating. In Fig. 2-(b), the interface between the nanostructured TiO_2 coating and the micron-sized $SrTiO_3$ core is marked with the white boundary line. Though the coating thickness varies with location, it is generally in the range of 40–80 nm, with the exception of occasional surface agglomerates attached through coalescence in the solution (see Fig. 2-(a)). The thickness is similar to that of dense TiO_2 films that exhibited substrate controlled, domain specific reactivity at the surface [13,14,39]. No obvious relationship between the annealing temperature and coating thickness was observed. $(Ba,Sr)TiO_3/TiO_2$ heterostructures annealed at all temperatures led to similar core–shell heterostructures.

The particle size of TiO_2 ranges from 50 nm to 80 nm, consistent with the XRD results. The coating annealed at 800 °C appears to be relatively dense, which is expected from a coating annealed at high temperatures (pore volumes will be discussed later). A high resolution TEM (HRTEM) image of a

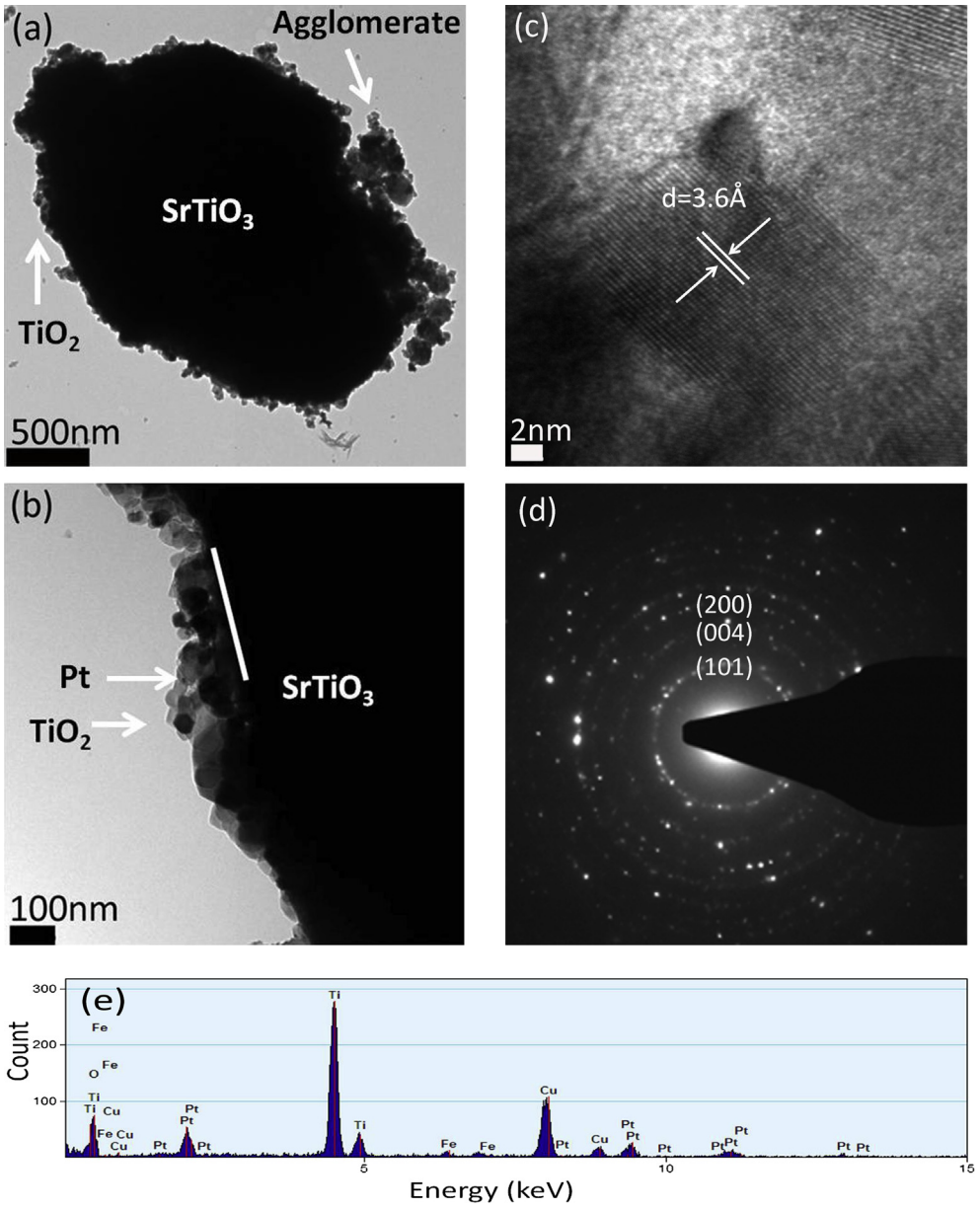

Fig. 2 – TEM analyses from a platinized heterostructured particle with *mc*-$SrTiO_3$/*ns*-TiO_2 shell annealed at 800 °C: bright field images (a) of the entire particle and (b) of the heterostructure interface, (c) a high resolution image of the *ns*-TiO_2 coating, (d) the SADP, and (e) an EDS spectrum from the coating.

TiO_2 coating is presented in Fig. 2-(c). The spacing between lattice fringes within the TiO_2 coating is measured to be 3.6 Å, corresponding to the (101) plane of anatase. The selected area diffraction pattern (SADP) of the TiO_2 coating is shown in Fig. 2-(d). The series of discrete concentric rings confirms the polycrystalline nature of the nano-sized grains. The diffraction rings were indexed and identified as anatase TiO_2. These observations are consistent with the XRD results. The diffraction spots observed outside the TiO_2 rings arise from the Pt co-catalyst; a Pt particle is highlighted in Fig. 2-(b). The presence of Pt was confirmed by EDS analysis in the STEM mode, as is shown in Fig. 2-(e). Cu and Fe peaks observed in the spectrum are introduced from the TEM specimen grid and lens pole-pieces. The thickness of the nanostructured coating is consistent with the previous reports that used the same experimental procedure [19,20].

The surface areas and pore volumes of all samples are summarized in Table 2. A pronounced inverse correlation exists between surface area and annealing temperature. The surface area of TiO_2 powder annealed at 800 °C is 1 m^2/g, indicating the TiO_2 particles (likely hard agglomerates of the ≈50 nm rutile grains) are micron-sized. The surface areas of the heterostructures also decrease with increasing annealing temperature, but with a much slower rate compared with TiO_2 alone. At annealing temperatures higher than 500 °C for $BaTiO_3$/TiO_2 and 600 °C for $SrTiO_3$/TiO_2, the surface area of the heterostructures is

Table 2 – Summary of physical properties of various photocatalysts annealed at different temperatures. (*S*: specific surface area; V_p: pore volume; $V_{H_2,6\,h}$: the total surface area specific volume of hydrogen after 6 h' photocatalysis reaction; and $R_{H_2,6\,h}$: hydrogen production rate per mass measured after 6 h' photocatalysis reaction. No hydrogen was detected from *mc*-$BaTiO_3$ and *mc*-$SrTiO_3$ without TiO_2 coating.)

Catalyst	Annealing temperature (°C)	S (m^2/g)	V_p (cm^3/g)	$V_{H_2,6\,h}$ ($\mu mol/m^2$)	$R_{H_2,6\,h}$ ($\mu mol(g\,h)^{-1}$)
TiO_2	400	93	0.19	11	171
	500	70	0.21	12	140
	600	16	0.06	18	48
	700	6	0.04	4	4
	800	1	0.004	0	0
$BaTiO_3/TiO_2$	400	72	0.15	9	108
	500	61	0.2	13	132
	600	44	0.14	28	205
	700	20	0.14	27	90
	800	15	0.09	18	45
$SrTiO_3/TiO_2$	500	47	0.16	22	172
	600	41	0.14	31	212
	700	22	0.13	12	44
	800	12	0.10	8	16
	900	7	0.02	0	0

larger than that of TiO_2 annealed at the same temperature. The surface area of micron-sized $BaTiO_3$ and $SrTiO_3$ is close to 1 m^2/g (not shown here). The decreased rate of pore collapse in the heterostructures indicates further (in addition to the phase and grain size observations) that core–shell interactions stabilize the nanoscale features of the shell.

The photocatalytic activity depends on the annealing temperature. In Table 2, the hydrogen produced per surface area after 6 h of photocatalytic reaction ($V_{H_2,6\,h}$) and the hydrogen production rate per mass ($R_{H_2,6\,h}$) are given for both heterostructured powders and unsupported TiO_2 annealed under various temperatures. A previous study of Pt-*mc*-$BaTiO_3$ and Pt-*mc*-$SrTiO_3$ showed that they produce little hydrogen because of their low surface area [21]. Several important points should be noted in these values with respect to an increase in temperature in the range of 400–600 °C. Over this range, the volume of hydrogen produced per surface area increases for all samples, with the heterostructures increasing more than the TiO_2 powders. $V_{H_2,6\,h}$ maximizes at 600 °C in the $SrTiO_3$($BaTiO_3$)/TiO_2 system at 31 (28) μmol m^{-2} and in TiO_2 at 18 μmol m^{-2}. The increase in the TiO_2 system likely comes from the increased crystallinity of the powders, though the variations in anatase/rutile fractions may also contribute. While both of these factors also contribute to the increase for the heterostructures, it is likely that the further improvement in photoreactivity for the heterostructures arises from improved bonding between the *ns*-TiO_2 coating and the *mc*-(Ba,Sr)TiO_3 core. Improved bonding facilitates carrier transfer between the *mc*-core and *ns*-shell [13,14,39], thereby increasing the available carriers for reaction in the *ns* shell for the *mc*-*ns* heterostructures compared to the *ns*-TiO_2.

The second important point to note for the reactivity from 400 to 600 °C relates to the combined effect of improved surface area stability and improved specific surface activity, as these two values multiplied together (and divided by the total reaction time) yield the mass specific rate of hydrogen production for each catalyst, $R_{H_2,6\,h}$ (μmol g^{-1} h^{-1}). For TiO_2, $R_{H_2,6\,h}$ dropped from 171 (400 °C) to 140 (500 °C) to 48 (600 °C) μmol g^{-1} h^{-1}, indicating the loss in overall surface area overwhelmed the modest improvement in reactivity per surface area. In contrast, the rate of hydrogen production per unit mass increased substantially for the heterostructures annealed at higher temperatures (up to 600 °C). For $BaTiO_3$/TiO_2 annealed at 400, 500, and 600 °C, $R_{H_2,6\,h}$ increased from 108 to 132 to 205 μmol g^{-1} h^{-1}, respectively. Similarly, for $SrTiO_3/TiO_2$ annealed at $T_A = 500$ and 600 °C, $R_{H_2,6\,h}$ increased from 172 to 212 μmol g^{-1} h^{-1}. These observations indicate that the improved reactivity per unit surface area for the heterostructures, related to strong interaction with the micron-sized cores, outweighs the surface area reduction owing to increased annealing temperatures (up to 600 °C). The improved mass specific rate is further helped in the heterostructures by the improved stability of the nanoscale coating, resulting in a decreased rate of surface area reduction with increased temperature. Overall, these observations demonstrate that nanoscale photocatalytic coatings can benefit greatly from interactions with micron-scale supports and light absorbing co-catalysts.

With a further increase in the annealing temperature, in the range of 700 °C–900 °C, the amount of hydrogen produced decreases for all samples measured by both $V_{H_2,6\,h}$ and $R_{H_2,6\,h}$. For TiO_2 at 700 and 800 °C, $V_{H_2,6\,h}$ (S) drops to 4 (6) and 0 (1) μmol m^{-2} (m^2/g) while $R_{H_2,6\,h}$ drops to 4 and 0 μmol g^{-1} h^{-1}. The drops in $V_{H_2,6\,h}$ and S indicate that changes in phase composition, grain size, and agglomerate size result in decreased efficiency for the net reactivity in the pure TiO_2 system. On the other hand, the hydrogen produced per surface area from $BaTiO_3/TiO_2$ annealed at 700 °C (27 μmol m^{-2}) is similar to the amount from the same heterostructure annealed at 600 °C (28 μmol m^{-2}), but the >50% reduction in surface area leads to a greater than 50% reduction in $R_{H_2,6\,h}$. A further increase in the annealing temperature to 800 °C causes a sharp reduction in the hydrogen produced per surface area (18 μmol m^{-2}), similar to that observed in the pure TiO_2

system. At this point the drastic drop in $R_{H_2,6\,h}$ comes from a combined loss of area specific hydrogen production and of total area. For $SrTiO_3/TiO_2$, the decrease in photocatalytic activity with annealing temperature above 600 °C is even more obvious than for $BaTiO_3/TiO_2$. The amount of hydrogen produced per surface area is only 12 μmol m^{-2} when annealed at 700 °C, a dramatic decrease from 31 μmol m^{-2} when annealed at 600 °C. With an annealing temperature of 900 °C, no hydrogen was detected. These observations indicate that, as the phase and nanostructure of the coating collapse, the improvements in the coating properties owing to the micron-scale core disappear. The fact that the $BaTiO_3$ retains high specific surface area reactivity to 700 °C suggests that the improved stability of anatase on $BaTiO_3$ extends the improvement in $V_{H_2,6\,h}$ to higher annealing temperatures. Finally, all of these results demonstrate that the heterostructures have an enhanced photocatalytic activity when compared with their components alone.

3.2. *Effect of coating thickness*

The thickness of the *ns*-shell was controlled by coating the core materials multiple times following identical procedures. TEM bright field images of $BaTiO_3/TiO_2$ coated once (BT-1), twice (BT-2), and three times (BT-3) (all annealed at 500 °C) are shown in Fig. 3(a)–(c). Most physical parameters, such as the crystal size of TiO_2, are similar between coatings with different cycles. The primary difference between these powders is simply the overall thicknesses of the coatings. Based on TEM images of the powders, the thickness of the TiO_2 layers resulting from two coatings was approximately 100–150 nm, or ≈twice as thick as what results from a single coating (40–80 nm). The thickness of TiO_2 coated three times is ≈150–250 nm, approximately three times the thickness of a single coating layer. The surface area and pore volume data of those powders are shown in Table 3. The increases in mass specific surface area and pore volume, with increased number of coating cycles, are small, but they are consistent with expectations for the thicker coatings having more nanostructured, high surface area TiO_2. Dark field TEM images of BT-1 and BT-3 are presented in Fig. 4 to illustrate the distribution of the Pt cocatalyst on the surface of the core/shell heterostructured powders. In this contrast mode, the Pt particles appear as bright spots because of their diffraction intensity; the coating and core structure are also apparent. The images illustrate that the Pt is well dispersed on the TiO_2 coating and has particles with diameters of approximately 5 nm.

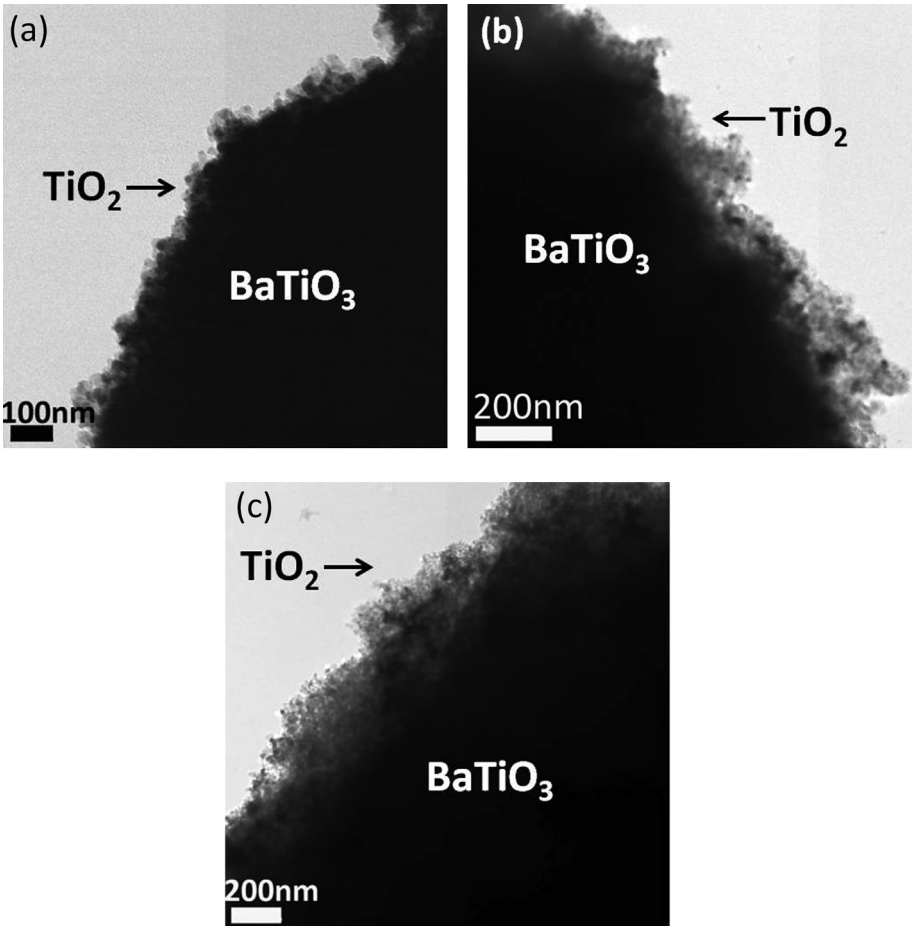

Fig. 3 – TEM bight field images of $BaTiO_3/TiO_2$ annealed at 500 °C with (a) one coating cycle, (b) two coating cycles, and (c) three coating cycles.

Table 3 – Summary of physical properties of $BaTiO_3/TiO_2$ annealed at 500 °C with different coating cycles. (BT-*n*: $BaTiO_3/TiO_2$ with *n* times coating cycles.)

Catalyst	S (m^2/g)	V_p (cm^3/g)	$V_{H_2,6\ h}$ ($\mu mol/m^2$)	$R_{H_2,6\ h}$ ($\mu mol(g\ h)^{-1}$)
BT-1	61	0.20	13	132
BT-2	64	0.25	17	181
BT-3	68	0.26	11	125

The photocatalytic activities of $BaTiO_3/TiO_2$ heterostructures with different coating thicknesses are shown in Table 3. Sample BT-2 ($BaTiO_3/TiO_2$ powders coated twice) produced more hydrogen per unit surface area and per gram-hour than samples BT-1 or BT-3. The value of 181 $\mu mol(g\ h)^{-1}$ observed for BT-2 is improved over the components alone (annealed at any temperature). It should be noted that these observations were made for samples annealed at 500 °C, below the optimal annealing temperature observed for samples coated once. Similar improvements are expected in samples annealed at other temperatures, though the optimal coating thickness may vary. That an optimal thickness is observed indicates that the heterostructure reactivity comes from an improvement in the nanoscale coating owing to interaction from the micron-scale core; this will be discussed later.

3.3. *Effect of Pt loading content*

The hydrogen production from heterostructured $SrTiO_3/TiO_2$ (coated once, annealed at 600 °C, and loaded with different Pt cocatalyst amounts) is shown in Fig. 5. The Pt loading varies from 0.1 wt% to 2 wt%. The $SrTiO_3/TiO_2$ powders loaded with 1 wt% Pt exhibit the highest photocatalytic activity for hydrogen production. In the range from 0.1 wt% to 1 wt%, the reactivity increases with Pt loading amount. Further increasing the loading to 2 wt% Pt results in a slight drop in reactivity. This phenomenon is consistent with a previous report on the effect of Pt loading on photocatalytic activity [40].

3.4. *Effect of core size*

A set of experiments was carried out to investigate the influence of the core size on the photocatalytic activity of the

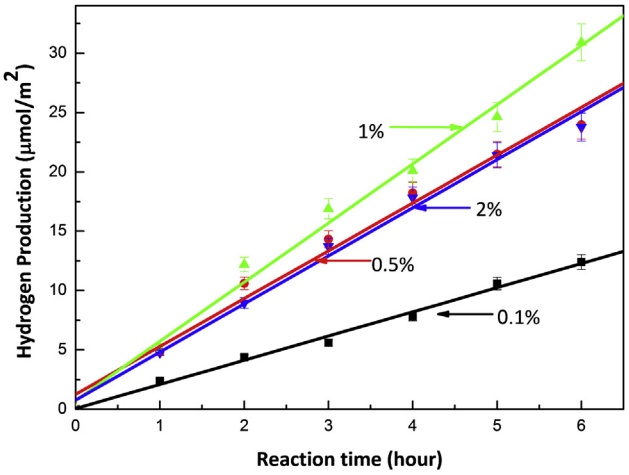

Fig. 5 – Hydrogen production from $SrTiO_3/TiO_2$ annealed at 600 °C with different Pt loading amounts. (The numbers marked in the figure refer to the weight percentage of Pt relative to the entire photocatalyst mass.)

heterostructures. Commercial $BaTiO_3$ nanoparticles were used as the core material (seeds in the sol–gel processing of TiO_2) and were coated with TiO_2 following the same procedure used to prepare the *mc*-$BaTiO_3$/*ns*-TiO_2. Table 4 contains the surface area and pore morphology data. The surface area of *ns*-$BaTiO_3$/*ns*-TiO_2 is 84 m^2/g, which is larger than the value of 61 m^2/g for *mc*-$BaTiO_3$/*ns*-TiO_2. Pore morphology parameters, other than surface area, did not change significantly.

The photocatalytic hydrogen production rate is shown in both Table 4 and Fig. 6. These photocatalysts were loaded with 1 wt% platinum. Based on the data, the hydrogen production rate from *mc*-$BaTiO_3$/*ns*-TiO_2 (132 $\mu mol\ g^{-1}\ h^{-1}$) is about 2.4 times that from *ns*-$BaTiO_3$/*ns*-TiO_2 (56 $\mu mol\ g^{-1}\ h^{-1}$). Moreover, *mc*-$BaTiO_3$/*ns*-TiO_2 produces 13 $\mu mol/m^2$, or about 3.3 times that produced per surface area of *ns*-$BaTiO_3$/*ns*-TiO_2, which was 4 $\mu mol/m^2$. Therefore, *mc*-$BaTiO_3$/*ns*-TiO_2 produced more hydrogen at a higher rate than *ns*-$BaTiO_3$/*ns*-TiO_2, even with a smaller surface area. No hydrogen was produced by *mc*-$BaTiO_3$ or *ns*-$BaTiO_3$ alone. While the low surface area of the uncoated particles may have contributed to this outcome, it is also consistent with the previous reports [41].

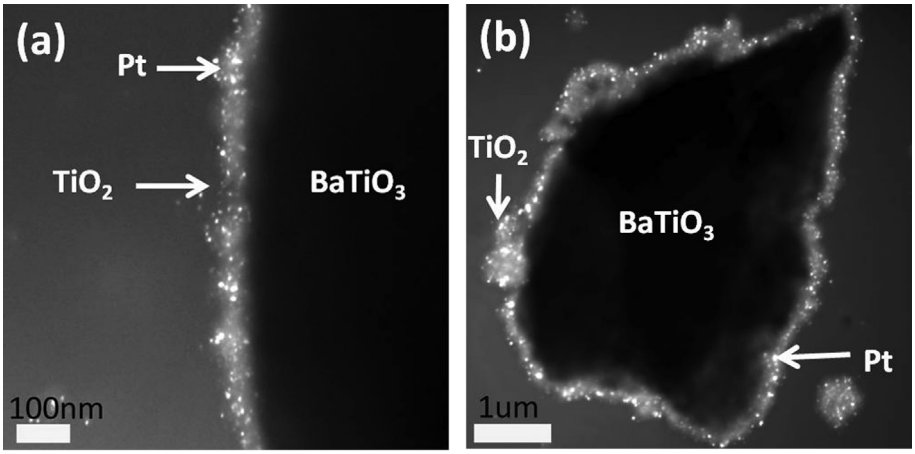

Fig. 4 – TEM dark field images of $BaTiO_3/TiO_2$ annealed at 500 °C with (a) one coating cycle, and (b) three coating cycles.

Table 4 – Physical properties of *mc*-$BaTiO_3$/*ns*-TiO_2 and *ns*-$BaTiO_3$/*ns*-TiO_2 annealed at 500 °C, as well as their components alone.

Composition	Surface area (m^2/g)	Pore volume (cc/g)	Pore radius Dv(r) (Å)	$V_{H_2,6\ h}$ μmol/m^2	R_{H_2} μmol g^{-1} h^{-1}
mc-$BaTiO_3$/*ns*-TiO_2	61	0.2	48	13	132
ns-$BaTiO_3$/*ns*-TiO_2	84	0.19	39	4	56
mc-$BaTiO_3$	0.8	0.003	16	0	0
ns-$BaTiO_3$	9	0.04	19	0	0

4. Discussion

The results described above indicate that the structural characteristics of the heterostructured catalysts affect hydrogen production. For the heterostructured powders, the photocatalytic activity per surface area initially increases with increasing annealing temperature and reaches a maximum at T_A = 600 °C. For unsupported TiO_2, the reactivity decreases continuously for higher annealing temperatures and lower surface areas. In the heterostructured catalyst, surface area alone is not the deciding factor. Because the titania shell is relatively thin compared to the absorption depth, the core absorbs most of the photons and transfers photo-excited charge carriers to the nanostructured shell [21]. Therefore, the structural integrity of the interface and the extent to which it allows charge transfer will influence the reactivity. High temperature annealing leads to improved shell crystallinity as well as interface properties. It is possible that the higher annealing temperature creates a more intimate contact, increasing the area of ordered, chemically bonded interface between the support and the titania, promoting charge transfer and contributing to enhanced photocatalytic activity. The sonomechanical mixture of $BaTiO_3$ and commercial TiO_2 did not show improved photocatalytic hydrogen production. This observation confirms the importance of the interface between the components [21]. This is the likely reason why the hydrogen produced from (Ba,Sr)TiO_3/TiO_2 heterostructures increases (from 108 μmol/(g h) to 205 μmol/(g h) for $BaTiO_3$/TiO_2) with annealing temperature from 400 °C to 600 °C, while unsupported TiO_2 shows a decrease in reactivity from 171 μmol/(g h) to 48 μmol/(g h) for the same range of annealing temperatures. In addition, improved crystallinity of the titania might also contribute to the increase in the photocatalytic activity per surface area for all photocatalysts with increasing temperature up to 600 °C. The crystallinity increases with temperature [9] and decreases the charge carrier recombination rate. Therefore, it is beneficial for photocatalytic hydrogen production.

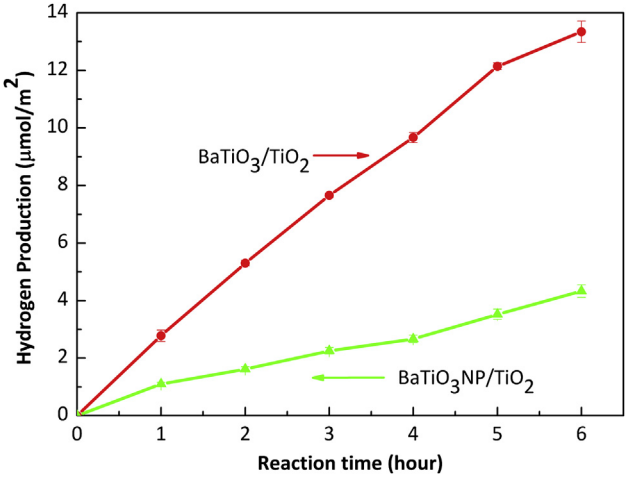

Fig. 6 – Hydrogen production from platinized *mc*-$BaTiO_3$/*ns*-TiO_2 ($BaTiO_3$/TiO_2) and *ns*-$BaTiO_3$/*ns*-TiO_2 ($BaTiO_3$NP/TiO_2) annealed at 500 °C.

The phase composition of the nanostructured TiO_2 coating also changes with annealing temperature. The percentage of anatase TiO_2 in the $BaTiO_3$/TiO_2 heterostructures decreases from 93.6% at 400 °C to 66.5% at 800 °C. It has been reported that anatase shows better photocatalytic activity than rutile under the same processing conditions [36]. The decrease in the amount of anatase TiO_2 is one reason for the decrease in photocatalytic reactivity per surface area of all photocatalysts above 600 °C. With an annealing temperature of 800 °C, TiO_2 did not even produce detectable amounts of hydrogen. Because of the support, the anatase content of $BaTiO_3$/TiO_2 did not change significantly from 600 °C to 700 °C. As a result, the amount of hydrogen production per surface area also remained constant. The transformation from anatase to rutile also leads to changes in light absorption. The absorption coefficients for anatase and rutile are 2×10^3/cm and 1×10^5/cm, respectively [13,42]. Rutile will absorb more light before it reaches the core and the charge carriers excited in this region of the catalyst will not be influenced by the space charge region in the core that separates electrons and holes and suppresses recombination.

The density of the titania coating also increases with annealing temperature. This has been shown by TEM images of $SrTiO_3$/TiO_2 annealed at 800 °C (Fig. 2) and further confirmed by the decrease in pore volumes with increasing annealing temperatures (Table 2). Denser coatings make the infiltration of the solution more difficult. Therefore, electrons from the microcrystalline core need to travel longer distances to the outer TiO_2 coating to reach the active sites. This is likely to increase the recombination rate of photogenerated charge carriers.

The results show that the heterostructure also retards both the phase transformation of anatase to rutile and the collapse of pores, thus maintaining a high surface area and high photocatalytic activity after elevated temperature annealing. As shown in Table 2, the (Ba,Sr)TiO_3/TiO_2 heterostructures show enhanced photocatalytic activities compared with TiO_2 alone for annealing temperatures greater than or equal to 600 °C. For catalysts annealed at 800 °C, (Ba, Sr)TiO_3/TiO_2 still catalyzes

the formation of measurable quantities of hydrogen while TiO_2 does not. All photocatalysts studied eventually experience a decrease in surface area and hydrogen production when the annealing temperature is large enough.

The annealing temperature influences the interface quality, phase composition, light absorption, crystallinity, mesoporosity and surface area. Furthermore, changes in the titania structure are likely to influence the distribution of Pt on the coating surface. Therefore, it is not possible to create a simple model relating annealing temperature to performance. The reason is that increased temperature in some cases promotes features beneficial to reactivity (interface quality and crystallinity) and in other cases promotes features detrimental to reactivity (densification and rutile content). Still, there is a temperature range around 600 °C wherein the performance can be optimized.

Titania shells produced by two coating cycles produced more hydrogen than those produced by a single coating or three coatings. This phenomenon can be explained in the following way. For the thinnest coatings, most of the light is absorbed in the space charge region of the core. The space charge at the buried interface promotes charge carrier separation and, depending on the local charge at the interface, electrons or holes are shuttled to the titania layer where they participate in redox reactions. Initially, increasing the coating thickness corresponds to increasing the number of active surface sites and, as a result, the amount of hydrogen produced increases. Sufficiently thick coatings are expected to act like bulk titania, and this was demonstrated by earlier work for the photochemical reduction of Ag [13]. The thickness of the depletion layer is estimated to be about 100 nm [2]. With a coating thickness larger than the depletion layer width, the bands relax to the bulk level in the center of the coating. In this case, the photocatalytic activity of $BaTiO_3/TiO_2$ should be identical to bulk TiO_2. This speculation is consistent with our experiment results. In Table 3, the amount of hydrogen produced per surface area from BT-3 (the number represents coating cycles) is about 11 μmol/m^2, which is very close to the value of TiO_2 alone (12 μmol/m^2). So, if the coating is too thick, the core provides no benefit.

The reactivity of heterostructured $SrTiO_3/TiO_2$ depends on the amount of Pt cocatalyst. The result shows that photocatalytic hydrogen production reached the maximum value when $SrTiO_3/TiO_2$ is loaded with 1% Pt. Enhanced photocatalytic hydrogen production from 0.1% to 1% (Pt wt%) can be attributed to the increase of active sites for hydrogen production. Higher amount of cocatalyst loading promotes Schottky barrier formation between TiO_2 and Pt, leading to the effective separation of charge carriers [40]. The phenomenon that the photocatalytic hydrogen production rate decreases with a further increase in Pt loading content to 2% is probably explained by agglomeration and growth of Pt nanoparticles on the $SrTiO_3$ surface [43]. In addition, Pt also promotes the reverse reaction of hydrogen and oxygen to form water [44].

We found that $BaTiO_3$ microcrystals coated with nanostructured TiO_2 show higher photocatalytic activity than the nanostructured $BaTiO_3$/nanostructured TiO_2 under the same processing conditions. The dimension of nano-sized $BaTiO_3$ is about 100 nm. In this size range, which is similar to the estimated space charge region, significant band bending is not permitted [2,45]. The spontaneous polarization also decreases substantially in the nanoscale range [22,46,47], leading to the decreased separation of photogenerated charge carriers in the core owing to ferroelectricity. Meanwhile, the dielectric constant of $BaTiO_3$ with the size of 100 nm is reported to be significantly smaller than the value for micron-sized $BaTiO_3$ [48]. The width of the space charge region is proportional to the dielectric constant; therefore, if the donor density is constant, a reduction in the dielectric constant shrinks the size of the space charge region in which charge carriers are separated. All three of these factors cited above suggest that smaller particles have reduced space charge regions, that fewer electron hole pairs will be separated (more will recombine), and that fewer photogenerated charge carriers are available for transfer to the TiO_2 coating where they can take part in a reaction. Therefore, reductions in particle size that reduce the space charge width are detrimental to the reactivity.

The energy level diagrams in Fig. 7 illustrate some of the points in the previous paragraph. These diagrams are modified from a previous report and the assumptions used for the placement of the energy levels are described in that reference [21]. In Fig. 7(a), we assume the ferroelectric polarization is suppressed in nanoscale $BaTiO_3$, and that the band bending regions associated with opposite surfaces overlap in the center of the structure. For the micron-sized cores (Fig. 7(b) and (c)), the band bending in the core is fully developed. Because

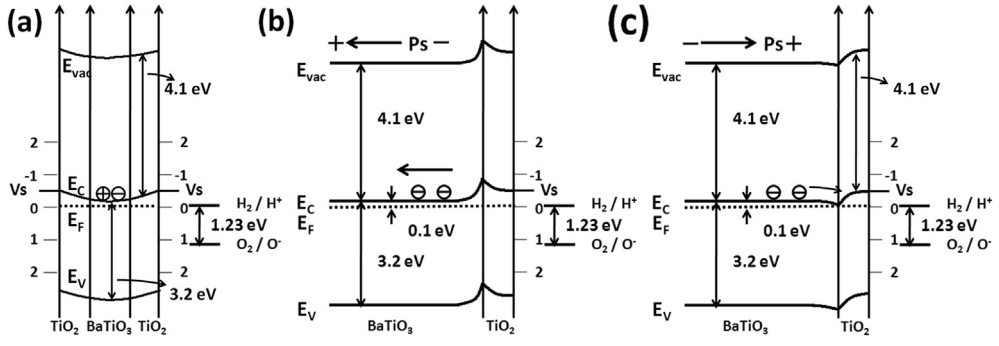

Fig. 7 – A highly simplified schematic representation of band structure diagram of heterostructured $BaTiO_3/TiO_2$ for: (a) *ns*-$BaTiO_3$/*ns*-TiO_2 and (b) (c) *mc*-$BaTiO_3$/*ns*-TiO_2 with different polarization directions. (E_{vac}, E_c, E_f and E_v represent the edge for vacuum level, conduction band, Fermi level and valance band, respectively. P_s refers to spontaneous polarization from ferroelectrics. The hydrogen and oxygen redox levels are shown in the right.)

most of the light is absorbed in this space charge region, decreased charge carrier recombination is expected. Also, internal fields in the heterostructures influence reactivity, as shown for the internal dipolar field in ferroelectric $BaTiO_3$ in Fig. 7(b) and (c). The ferroelectric polarization from the micron-sized core will influence the band bending at the interface between the core and shell and assist the separation of photogenerated charge carriers, as the schematics illustrate, as well as separating reactions locally at the surface.

The photocatalytic activity enhancement of *mc*-$BaTiO_3$/*ns*-TiO_2 is attributed to the photogenerated charge carrier separation in the micron-sized core, efficient charge transfer from the core to the shell through the interface, and the high surface area for reactivity in the nanostructured coating [21]. The absorption in $BaTiO_3$ and charge transfer from $BaTiO_3$ to TiO_2 was confirmed in earlier studies of planar heterostructures [13,14,39]. $SrTiO_3$ is known to exhibit similar internal fields near the surface that affect reactivity [17]. This discussion leads to the conclusion that the size dependence of the band bending, dielectric constant, and spontaneous polarization are likely to be responsible for the difference in photochemical activity between heterostructures with micron-sized core and with nanostructured core.

The results presented here demonstrate the superiority of microcrystalline core/nanostructured shell design over the nanocrystalline core/nanostructured shell design. According to the above argument, the ideal core would have the minimum size to sustain full polarization, dielectric constant, and band banding and that would absorb a significant number of photons. Optimization of the core-size has not been carried out in the current work.

5. Conclusions

mc-(Ba,Sr)TiO_3/*ns*-TiO_2 heterostructures produced more photocatalytic hydrogen than TiO_2 for processing temperatures between 500 °C and 800 °C. The hydrogen production rate of the heterostructured powders initially increased with annealing temperature, which is the opposite of what happens for TiO_2 alone. The maximum photocatalytic activity for hydrogen production was found for the heterostructures annealed at 600 °C. Further increases in the annealing temperature decrease the photocatalytic activity. Heterostructured *mc*-(Ba,Sr)TiO_3/*ns*-TiO_2 catalysts coated twice with titania produced more hydrogen than those coated once and three times. The heterostructures coated three times have properties comparable to bulk titania. Cocatalyst loading also influences photocatalytic hydrogen production. $SrTiO_3$/TiO_2 with 1 wt% Pt loading has the highest reactivity. Heterostructured catalysts with microcrystalline cores have a higher photocatalytic activity and those with 100 nm cores, suggesting that a minimum core size is needed.

Acknowledgments

This work was supported by the National Science Foundation (DMR 1206656) and the PA DCED.

REFERENCES

[1] Domen K. Characterization of photoexcitation processes on solid surfaces. In: Anpo M, editor. Surface photochemistry. Chichester: J. Wiley & Sons; 1996. p. 1–18.
[2] Albery WJ, Philip NB. The transport and kinetics of photogenerated carriers in colloidal semiconductor electrode particles. J Electrochem Soc 1984;131:315–25.
[3] Nozik AJ. Photoeffects at semiconductor-electrolyte interfaces. Washington, D.C.: American Chemical Society; 1981.
[4] Maeda K, Teramura K, Lu D, Saito N, Inoue Y, Domen K. Noble-metal/Cr_2O_3 core/shell nanoparticles as a cocatalyst for photocatalytic overall water splitting. Angew Chem Int Ed 2006;45:7806–9.
[5] Maeda K, Teramura K, Lu D, Saito N, Inoue Y, Domen K. Roles of Rh/Cr_2O_3 (core/shell) nanoparticles photodeposited on visible-light-responsive $(Ga_{1-x}Zn_x)(N_{1-x}O_x)$ solid solutions in photocatalytic overall water splitting. J Phys Chem C 2007;111:7554–60.
[6] Huang HJ, Li DZ, Lin Q, Shao Y, Chen W, Hu Y, et al. Efficient photocatalytic activity of PZT/TiO_2 heterojunction under visible light irradiation. J Phys Chem C 2009;113:14264–9.
[7] Zhang X, Zhang L, Xie T, Wang D. Low-temperature synthesis and high visible-light-induced photocatalytic activity of BiOI/TiO_2 heterostructures. J Phys Chem C 2009;113:7371–8.
[8] Pan J, Liu G, Lu GQ, Cheng H-M. On the true photoreactivity order of {001}, {010}, and {101} facets of anatase TiO_2 crystals. Angew Chem Int Ed 2011;50:2133–7.
[9] Kudo A, Miseki Y. Heterogeneous photocatalyst materials for water splitting. Chem Soc Rev 2009;38:253–78.
[10] Liu G, Yu JC, Lu GQ, Cheng H-M. Crystal facet engineering of semiconductor photocatalysts: motivations, advances and unique properties. Chem Commun 2011;47:6763–83.
[11] Chen X, Shen S, Guo L, Mao SS. Semiconductor-based photocatalytic hydrogen generation. Chem Rev 2010;110:6503–70.
[12] Inoue Y, Okamura M, Sato K. A thin-film semiconducting TiO_2 combined with ferroelectrics for photoassisted water decomposition. J Phys Chem 1985;89:5184–7.
[13] Burbure NV, Salvador PA, Rohrer GS. Photochemical reactivity of titania films on $BaTiO_3$ substrates: origin of spatial selectivity substrates. Chem Mater 2010;22:5823–30.
[14] Burbure NV, Salvador PA, Rohrer GS. Photochemical reactivity of titania films on $BaTiO_3$ substrates: influence of titania phase and orientation. Chem Mater 2010;22:5831–7.
[15] Zhang Y, Schultz AM, Salvador PA, Rohrer GS. Spatially selective visible light photocatalytic activity of TiO_2/$BiFeO_3$ heterostructures. J Mater Chem 2011;21:4168–74.
[16] Schultz AM, Salvador PA, Rohrer GS. Enhanced photochemical activity of a-Fe_2O_3 films supported on $SrTiO_3$ substrates under visible light illumination. Chem Commun 2012;48:2012–4.
[17] Giocondi JL, Rohrer GS. Structure sensitivity of photochemical oxidation and reduction reactions on $SrTiO_3$ surfaces. J Am Ceram Soc 2003;86:1182–9.
[18] Yeredla RR, Xu H. Incorporating strong polarity minerals of tourmaline with semiconductor titania to improve the photosplitting of water. J Phys Chem C 2008;112:532–9.
[19] Gao B, Kim YJ, Chakraborty AK, Lee WI. Efficient decomposition of organic compounds with $FeTiO_3$/TiO_2 heterojunction under visible light irradiation. Appl Catal B Environ 2008;83:202–7.
[20] Li L, Zhang Y, Schultz AM, Liu X, Salvador PA, Rohrer GS. Visible light photochemical activity of heterostructured

$PbTiO_3$-TiO_2 core-shell particles. Catal Sci Tech 2012;2:1945–52.
[21] Li L, Rohrer GS, Salvador PA. Heterostructured ceramic powders for photocatalytic hydrogen production: nanostructured TiO_2 shells surrounding microcrystalline (Ba,Sr)TiO_3 cores. J Am Ceram Soc 2012;95:1414–20.
[22] Akdogan EK, Rawn CJ, Porter WD, Payzant EA, Safari A. Size effects in $PbTiO_3$ nanocrystals: effect of particle size on spontaneous polarization and strains. J Appl Phys 2005;97:084305.
[23] Yashima M, Hoshina T, Ishimura D, Kobayashi S, Nakamura W, Tsurumi T, et al. Size effect on the crystal structure of barium titanate nanoparticles. J Appl Phys 2005;98:014313.
[24] Giocondi J, Salvador P, Rohrer GS. The origin of photochemical anisotropy in $SrTiO_3$. Top Catal 2007;44:529–33.
[25] Giocondi JL, Rohrer GS. The influence of the dipolar field effect on the photochemical reactivity of $Sr_2Nb_2O_7$ and $BaTiO_3$ microcrystals. Top Catal 2008;49:18–23.
[26] Li S, Lin YH, Zhang BP, Li JF, Nan CW. $BiFeO_3$/TiO_2 core-shell structured nanocomposites as visible-active photocatalysts and their optical response mechanism. J Appl Phys 2009;105:054310.
[27] Ye M, Zhang Q, Hu Y, Ge J, Lu Z, He L, et al. Magnetically recoverable core-shell nanocomposites with enhanced photocatalytic activity. Chem Eur J 2010;16:6243–50.
[28] Vorontsov AV, Stoyanova IV, Kozlov DV, Simagina VI, Savinov EN. Kinetics of the photocatalytic oxidation of gaseous acetone over platinized titanium dioxide. J Catal 2000;189:360–9.
[29] He ZQ, Xie L, Tu JJ, Song S, Liu WP, Liu ZW, et al. Visible light-induced degradation of phenol over iodine-doped titanium dioxide modified with platinum: role of platinum and the reaction mechanism. J Phys Chem C 2010;114:526–32.
[30] Kato H, Kudo A. Visible-light-response and photocatalytic activities of TiO_2 and $SrTiO_3$ photocatalysts codoped with antimony and chromium. J Phys Chem B 2002;106:5029–34.
[31] Chan CK, Porter JF, Li YG, Guo W, Chan CM. Effects of calcination on the microstructures and photocatalytic properties of nanosized titanium dioxide powders prepared by vapor hydrolysis. J Am Ceram Soc 1999;82:566–72.
[32] Shi J, Chen J, Feng Z, Chen T, Lian Y, Wang X, et al. Photoluminescence characteristics of TiO_2 and their relationship to the photoassisted reaction of water/methanol mixture. J Phys Chem C 2007;111:693–9.
[33] Porter JF, Li YG, Chan CK. The effect of calcination on the microstructural characteristics and photoreactivity of Degussa P-25 TiO_2. J Mater Sci 1999;34:1523–31.
[34] Wu NL, Lee MS, Pon ZJ, Hsu JZ. Effect of calcination atmosphere on TiO_2 photocatalysis in hydrogen production from methanol/water solution. J Photochem Photobiol A Chem 2004;163:277–80.
[35] Gao L, Zhang QH. Effects of amorphous contents and particle size on the photocatalytic properties of TiO_2 nanoparticles. Scripta Mater 2001;44:1195–8.
[36] Hurum DC, Agrios AG, Gray KA, Rajh T, Thurnauer MC. Explaining the enhanced photocatalytic activity of Degussa P25 mixed-phase TiO_2 using EPR. J Phys Chem B 2003;107:4545–9.
[37] Kozlova EA, Korobkina TP, Vorontsov AV, Parmon VN. Enhancement of the O_2 or H_2 photoproduction rate in a Ce^{3+}/Ce^{4+}-TiO_2 system by the TiO_2 surface and structure modification. Appl Catal A Gen 2009;367:130–7.
[38] Cullity BD, Stock SR. Elements of X-ray diffraction. MA: Addsion-Wesley Publishing Co; 1978.
[39] Burbure NV, Salvador PA, Rohrer GS. Influence of dipolar fields on the photochemical reactivity of thin titania films on $BaTiO_3$ substrates. J Am Ceram Soc 2006;89:2943–5.
[40] Yi H, Peng T, Ke D, Ke D, Zan L, Yan C. Photocatalytic H_2 production from methanol aqueous solution over titania nanoparticles with mesostructures. Int J Hydrogen Energy 2008;33:672–8.
[41] Yamashita Y, Tada M, Kakihana M, Osada M, Yoshida K. Synthesis of RuO_2-loaded $BaTi_nO_{2n+1}$ ($n = 1$, 2 and 5) using a polymerizable complex method and its photocatalytic activity for the decomposition of water. J Mater Chem 2002;12:1782–6.
[42] Park YR, Kim KJ. Structural and optical properties of rutile and anatase TiO_2 thin films: effects of Co doping. Thin Solid Films 2005;484:34–8.
[43] Hwang DW, Kim HG, Kim J, Cha KY, Kim YG, Lee JS. Photocatalytic water splitting over highly donor-doped (110) layered perovskites. J Catal 2000;193:40–8.
[44] Osterloh FE. Inorganic materials as catalysts for photochemical splitting of water. Chem Mater 2008;20:35–54.
[45] Kavan L, Grätzel M, Gilbert SE, Klemenz C, Scheel HJ. Electrochemical and photoelectrochemical investigation of single-crystal anatase. J Am Chem Soc 1996;118:6716–23.
[46] Li XP, Shih WH. Size effects in barium titanate particles and clusters. J Am Ceram Soc 1997;80:2844–52.
[47] Asiaie R, Zhu W, Akbar SA, Dutta PK. Characterization of submicron particles of tetragonal $BaTiO_3$. Chem Mater 1996;8:226–34.
[48] Shaw TM, Trolier MS, McIntyre PC. The properties of ferroelectric films at small dimensions. Annu Rev Mater Sci 2000;30:263–98.